Evidence of Elliptical Intrusions and Sr, Hf, Pb, O Isotopes of the Khanbogd Alkali Granite Pluton: Constraction of Under-plating Magma Associated with the Duplex Thrust

DASH BATULZII * , HOLK GREGORY , SERJLKHUMBE AMARAMGALAN

Posted Date: 16 January 2024

doi: 10.20944/preprints202401.1242.v1

Keywords: alkali granite; satellite image; elliptic shape; δ18O isotope; duplex thrust; underplating

Article

Evidence of Elliptical Intrusions and Sr, Hf, Pb, O Isotopes of the Khanbogd Alkali Granite Pluton: Constraction of Underplating Magma Associated with the Duplex Thrust

Dash Batulzii [1,*], Holk Gregory [2], Serjlkhumbe Amaramgalan [3], Otgonhuu Javkhlan [1] and Davaa Khishigsuren [1]

[1] School of Geology and Mining Engineering, Mongolian University Science and Technology, Ulaanbaatar 14191, Mongolia; ulziid59@gmail.com
[2] Department of Geology, Californian State University Long Beach, Long Beach, CA 90840, USA; gregory.holk@csulb.edu
[3] Rio Tinto Company, London SW1Y 4AD, UK; AmaramgalanS@riotinto.com
* Correspondence: ulzii@must.edu.mn; Tel.: +976-99243602

Abstract: The studied Khanbogd pluton of peralkaline granite is located in southern Mongolia and occupies an area of ~1000 sq. km. Previously, two ring-shaped bodies were constructed in a flattened shape pluton. However, this shape was not used for the genesis of this pluton. A recent study of Landsat image showed a several elliptical intrusions in two bodies. Chemistry interpretation shows that each intrusion differs in ASI, CIPW norms, $^{87}Sr/^{86}Sri$ and δ18O isotopes. Elliptical intrusions, uplifted country rocks between them, and roof pendants suggest magma penetration along fractured country rocks. Furthermore, two adjacent intrusive bodies and undeformed host rocks at the front part of the pluton are consistent with underplating magmatic factors during duplex-type thrusting. This magma event is also supported by low of Sr, Ba, Eu and high of Th, U, Pb anomalies and a few amount of garnet crystals in the granites, implying vapor absent melt crystallization associated with underplating. Multiple melt sources, as well as from mantle and recycled sea floor rocks, are identified by ratio of 87Sr /86Sri and δ18O values. The low isotope values, the thrust nature and 295–286 Ma ages of the alkali granites, indicate an underplate magma evidenced during Permian rifting.

Keywords: alkali granite; satellite image; elliptic shape; $\delta^{18}O$ isotope; duplex thrust; underplating

1. Introduction

It is widely known that the geology of Mongolia is characterized by the accretion of arc complexes and accompanying voluminous calc-alkaline granites e.g., [25]. However, alkaline granites are present and some are very impressive. One of them is Khanbogd peralkaline granite pluton that occurs in Southern Mongolia. The impressive feature of this pluton is its size, occupying over 1000 sq. km, amazing outcrop shapes and pegmatites containing REE mineralization. The granitoid phases and their geochemistry of this pluton have been studied by Russian scientists e.g., [30,63]. At the beginning stage of studying this pluton, three-phase granites, various composition dikes and REE bearing permatites were identified in two adjasent ring-shaped intrusive bodies [63]. The study by Kovalenko et al. [30] not only revised previous materials, but also introduced new data on the age of zircon and the flattened shape of the pluton based on modeling of gravity data. However, this shape was not used for the genesis of the pluton. The ring or circulation form of the pluton, presumably resulting from the magma ascending, was introduced by the Mongolian researcher Garamzhav e.g., [16]. A giant pluton composed of alkaline granites in two bodies, exhibiting low Sr, Hf, Pb isotopic values, as well as wall rock pendants in the top of granite outcrops motivate us to find some connection with the flattened shape of this pluton. On the other hand, we had an interest in analyzing the geochemical and isotopic data from Serjlkhumbe [48,49] that was not published related to her new job at a mining company. We therefore began to interpret

 doi:10.20944/preprints202401.1242.v1

Landsat satellite images of the Khanbogd pluton. At least we interpreted several elliptical intrusions within the two bodies that were named western and eastern by the previous researchers [30,63].

The position of the previously collected samples provided us with the opportunity to examine chemical and isotopic data according to interpreted intrusions. In addition, the various amount of garnet in association with aegirine and arfvedsonite in all granites led us to consider experimental data of Patino Douce [44]. The result of his experiment was similar to the experimental data obtained from e.g., [7,18,53], that is, the alkaline and leucogranites are derived from the melting of tonalite, granite gneiss and pelite. The flattened shape of this pluton [30] and new data on 87Sr/86Sr - δ18O ratios required us to reconsider the magma model associated with thrusting, which involved the melting of mantle and modified oceanic rocks. These tasks were provided by the underplating melt, accompanied by duplex-type thrusts. Therefore, this manuscript presents our interpretation of satellite images of the Khanbogd pluton, petrographic, geochemical, isotopic data (Sr, Nd, Hf, Pb and O) of alkaline granites, as well as a new model of the giant Khanbogd alkaline pluton.

2. Materials and Methods

Quartz $\delta^{18}O$ values were measured using the Thermo Finnigan Delta Plus-XP mass spectrometer at California State University, Long Beach. A modified version of the laser fluorination method of Sharp [52] and the TC/EA method e.g., [51] was employed for the acquisition of quartz $\delta^{18}O$ values, respectively. Analytical precision and accuracy for oxygen ($\delta^{18}O \pm 0.2‰$) isotopes were determined using the NBS-30 biotite (Caltech Rose Quartz ($\delta^{18}O = +8.45‰$) e.g.,[17,56], standards and reported relative to V-SMOW. Whole rock major and 14 trace element (Ba, Ce, Cr, Ga, Nb, Ni, Pb, Rb, Sc, Sr, Th, V, Y, Zr) concentrations for 35 samples were analyzed by Rigaku RIX-2000 wavelength-depressive XRF spectrometer at Shimane University e.g., [49]. REEs, Cs, Rb, Ba, Sr, Th, U, Nb, Ta, Pb, Zr, Hf, Li, and Y analyses were carried out for selected samples by ICP-MS (Thermo ELEMENTAL, VGPQ3 at Shimane University), following the method described by Kimura et al. [27]. Sr and Nd isotopic ratios were determined for 36 samples by thermal ionization mass spectrometry (MAT262) at Shimane University, following the methods described in [23,24]. The isotopic compositions were measured in jumping multi-collection mode. The Sr isotope ratios of standard sample NBS987 ($SrCO_3$) were used during the analysis. Sr isotope compositions and age dating were determined by isotope dilution method due to the very high Rb/Sr values and very low average Sr concentrations (<10 ppm) of the Khanbogd plutonic complex. Samples were mixed with spike solution ($^{87}Rb/^{86}Sr$ mixed spike, which was previously prepared at Shimane University of Japan).

3. Geological background of the studied Khanbogd alkali granite pluton

3.1. Geological, mineralogical studies of the previous and proposed ones in the Khanbogd pluton and its surroundings

The studied Khanbogd pluton is located in the south of southern Mongolia (Figure 1). This pluton intruded into the Lower Carboniferous sedimentary basin filled by the volcano-sedimentary strata e.g., [30]. According to the terrane-tectonic concept, this basin is located near the southern accretion zone of the Gurvansaikhan terrane e.g.,[2], (Figure 1). Geological studies of alkaline granites of the Khanbogd pluton began in 1970-1980, the first results were summarized by Vladykin et al. [63]. Accordingly, the Khanbogd pluton is represented by aegirine-arfvedsonite alkaline granites in two intrusive bodies: western (~1000 km^2) and eastern (~300 km^2) e.g.,[63]. At the beginning of the studies, 3 phase granites were identified for the western body, represented by coarse-medium, medium-fine-grained aegirine-arfvedsonite granites, including smaller size red granites. For the eastern body, medium-grained aegirine-arfvedsonite and fine-grained aegirine granites were described e.g.,[63].

 doi:10.20944/preprints202401.1242.v1

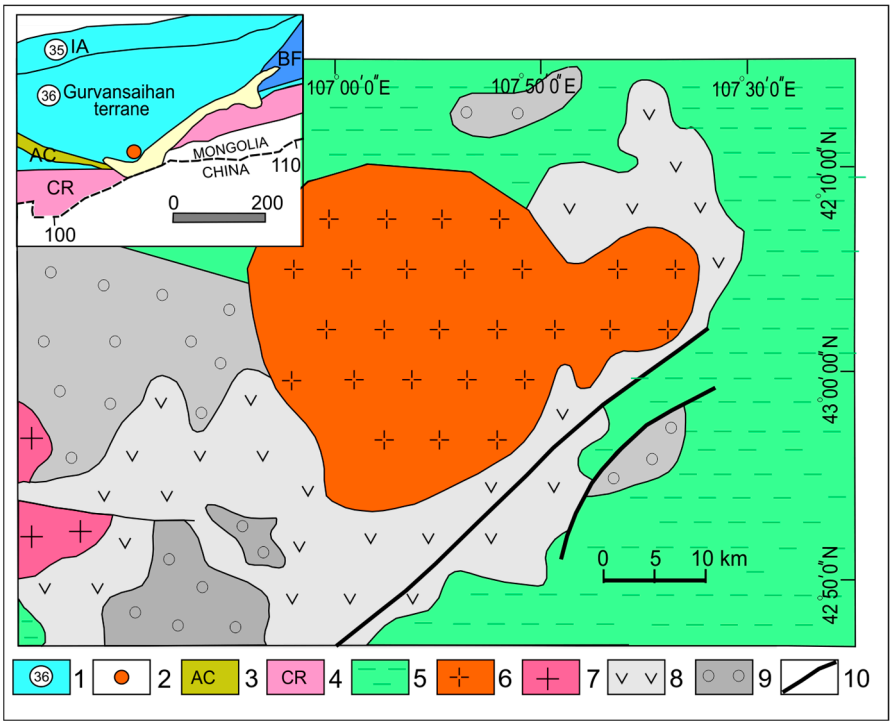

Figure 1. A location of Khanbogd plutonic complex in the terrane tectonic scheme of Mongolia and geological units in the pluton and its surroundings. Modified from [2,68]. 1- Gurvansaihan island arc terrane (36) in southern Mongolia e.g.,[2], 2- locality of Khanbogd peralkaline granite pluton in Gurvansaihan terrane, 3- accretionary wedge (AC), 4-cratonal terrane (CR), 5-Lower and Upper Cretaceous coarse grained reddish sedimentary formation; 6- Early Permian, Khanbogd alkaline granite plutonic complex, 7-Early Permian leucogranite intrusions, 8- Lower Carboniferous andesite and dacite dominant volcanic unit, 9- Lower Carboniferous sedimentary clastic unit with volcanic beddings, 10- part of terrane bounding fault.

Numerous REE bearing pegmatites and various compositions of dikes, as ekerite, pantellerite, and comendites-were identified in the pluton e.g.,[63]. Elpidite ($Na_2Zr_6Si_6O_{15}$ H_2O) is a specific accessory mineral in these granites and pegmatites e.g.,[63]. In addition, the zirconium oxides as armstrongite ($CaZrSi_6O_{15}$ $3H_2O$) and mongolite ($Na_2ZrSi_6O_{15}$ $3H_2O$) were discovered by the Vladykin e.g., [62,64] in pegmatites. The study by Kovalenko et al. [30] not only revised previous materials, but also introduced U/Pb zircon ages, Sr isotopes of alkaline granites and the flattened shape of the pluton based on modeling of gravity data [29,30].

Accordingly, the phases were integrated, and instead of them, granites were recorded by grain size: coarse-medium-grained granites in the western body and medium-fine-grained granites in the eastern body e.g., [30]. The work of Serjlkhumbe e.g., [49] showed that the small intrusions of red granite contain ferro-edinite. U/Pb zircon ages from 291±1 to 290±1 Ma and Rb/Sr age of 287±3 Ma for granites of the western body were received by Kovalenko et al.[28]. However, Serzhlkhumbe e.g., [49] obtained Rb/Sr ages of 295–292 Ma from aegirine-arfvedsonite granites or granites and dikes.

In the surrounding area of the Khanbogd pluton, Lower Carboniferous volcanic-sedimentary strata are intruded by Early Permian intrusions and overlained by the Lower and Upper Cretaceous, red sediments, characteristic of the geology of Southern Mongolia (Figure 1), e.g., [68]. Early Permian formations are represented by basalt-comendites of the bimodal series volcanic rocks e.g.,[70]. In the basin where the Khanbogd pluton is located, leucogranites, which are analogues of felsic lava of bimodal series volcanite, are widespread (Figure 1).

 doi:10.20944/preprints202401.1242.v1

3.2. Interpretation of landsat satellite images and the elliptic intrusions of alkaline granite units in the Khanbogd pluton

In particular, for interpretation we used a combination of "Landsat" spectral bands 2-3-4, 4-5-1, 5-3-2 and 7-4-1. Four shapes, identical to the phases, are represented by different color images across the western body (Figures 2a-2d). The yellowish, pale red- pinkish, bluish and pale pinkish color (Figures 2a-2d) tones are reflected from a strip of arcuate shape that is in the outer margin of the western body. This is marked I-W in Figure 2e, defining the first phase intrusion of the western body. An elliptical shape inside the arcuate strip is noted II-W (Figure 2e), reflects pale bluish-gray, bluish, brownish and pale reddish phototones (Figures 2a-2d). A narrow blackish zone is distinguished between an elliptical (II-W) and an arcuate shape (I-W) shapes (Figures 2a-2d). This zone represents uplifted wall rocks and indicates a boundary of two-phase granites. The smaller figure, displayed by dark and pale blue (Figure 2a, 2b), brown (Figure 2c), bright reddish (Figure 2d) phototons, is the next phase in the relationship and is noted III-W (Figure 2e). Images marked IV-W (Figure 2e) refer to small intrusions of ferro-edenite granites. Dikes of ferro-edinite granites are common in III-W. Satellite images display a sharp contact between the western and eastern intrusive bodies. The cross-cutting relationships between granites indicates that the eastern small elliptical body is younger than the western. Contrasting colors in the small body suggest there are two units in eastern body and marked as the I-E and II-E (Figure 2e). A smaller unit that displays images similar to IV-W and has many pendants is considered younger and marked II-E (Figure 2e). The granites I-E, which occupy most part of the eastern body, illustrate the lighter images (Figures 2a-2e). Interpreted elliptical figures representing phase intrusions in the studied Khanbogd pluton are shown in Figure 2e.

 doi:10.20944/preprints202401.1242.v1

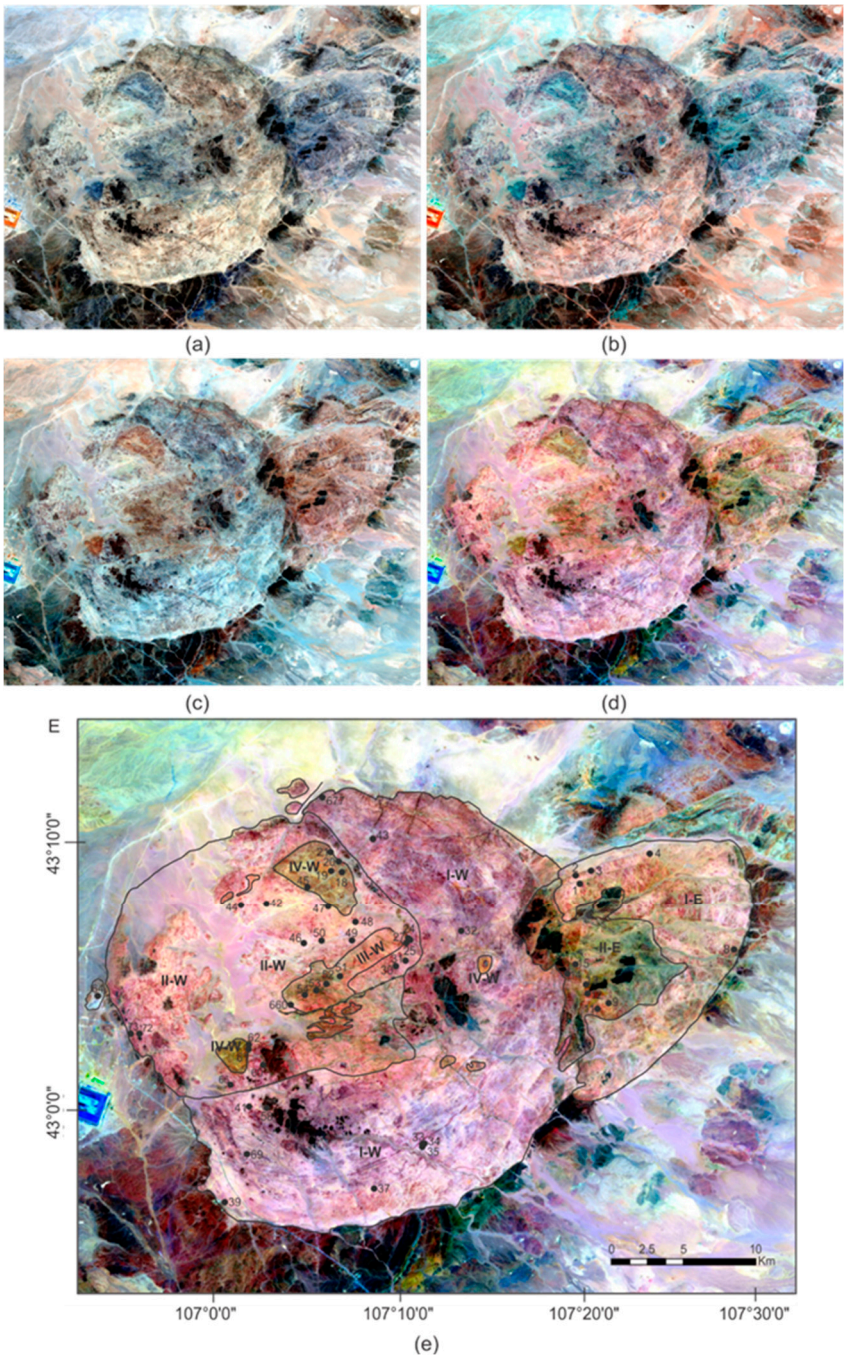

Figure 2. Images of the Khanbogd granite pluton in the Landsat bands and an interpreted map using them. Landsat bands: (a)- /2-3-4; (b)- /4-5-1/; (c)- /5-3-2/; (d)- /7-4-1/; (e) interpreted schematic map and sample points (Interpretation by Batulzii, Holk and Bayartsengel).

3.3. Texture of granite outcrops of distinguished intrusions, their relationships, dikes, roof pendant and mineralization

The above-mentioned intrusions differ primarily in the texture of their outcrops. For example, granite outcrops of the I-W are characterized by a spheroidal weathering on Earth surface. The shapes were formed by intersecting joints (Figure 3a). This arcuate-shaped, I-W intrusion is mostly composed of coarse-grained, porphyritic and agpaitic aegirine-arfvedsonite granites (Figure 3b). The outcrops of II-W are characterized by vertical joints that were intersected by shallow-dipping, closer-spaced joints (Figure 3c).

 doi:10.20944/preprints202401.1242.v1

Figure 3. Outcrop and hand specimen photos of alkali granites in western body Khanbogd pluton. (a)- outcrop of unit I-W, (b)- course grained porphyritic texture greyish color aegirine-arfvedsonite granite in I-W, (c)- outcrop of unit II-W, where dominated horizontal platy joint, (d)- elpidite rich agpaitic, greyish color granite in II-W, (e)-outcrop of unit III-W, intruded into unit II-W, (f)-reddish color aegirine-arfvedsonite granite in unit III-W, (g)- outcrop of unit IV-W, where cubic shape is formed from set of vertical and horizontal joints, (h)- red color, ferro-edinite granite.

Intrusion II-W is represented by pale pink, medium-to-coarse-grained, equigranular and porphyritic, aegirine-arfvedsonite granites (Figure 3d). The elpidite content locally exceeds the other

 doi:10.20944/preprints202401.1242.v1

accessory minerals (Figure 3d). The outer contact zone II-W is not only controlled by the uplifted host rocks (Figure 2e) but also by banded pegmatite zones with quartz cores. The outcrops III-W are characterized by a rough, fractured surfaces. Spheroids were destroyed by dikes of IV-W. The outcrop area of this unit was documented by Kovalenko et al.[29], but the compositional character has not been studied. The contact where III-M intrudes II-M is clearly visible by their colors and shapes (Figure 3e). The intrusion III-M is composed of brown-reddish medium-grained aegirine-arfvedsonite granites (Figure3f). Outcrops IV-M are distinguished from others by their reddish color and shape, formed by intersecting vertical and horizontal sets of joints (Figure 3g). These red porphyritic granites have plagioclase phenocrysts, along K-feldspar and ferro-edinite (Figure 3h).

As mentioned above, two intrusions have been identified within the eastern body. Fine-grained red aegirine-arfvedsonite granite II-E formed between I-W and I-E. The blackish color reflected from the red granite outcrops is explained by the scattered pendant fragments resulting from thin pendant (Figure 4a). Their apophases to I-W and I-E demonstrate its younger generation (Figs.4a, 4b). Granites II-E are characterized by aegirine and red K-feldspar phenocrysts embedded in a fine-grained reddish groundmass (Figure 4c). The older one (I-E) is characterized by the medium grained spherical-textured lilac granites (Figure 4c), where pinkish K-feldspar phenocrysts are in lilac ground mass (Figure 4d).

The various composition of dikes is associated with the Khanbogd pluton. For instance, sub-parallel ekerite dikes and pegmatites with arfvedsonite and elpidite occur in the arc-shaped intrusion. Red comendite dikes with large K-feldspar phenocrysts are common in granites II-W (Figure 4e). Dark gray pantellerite dikes and elpidite-bearing pegmatites are described from intrusions II-W and III-W (Figure4f).

In accordance with the identification of several intrusions, we revise the location of REE mineralization. The horizontal shape pegmatites that consist mainly of large crystals of arfvedsonite-elpidite pegmatites are occur the southern part of arcuate shape I-W intrusion body (Figure 4g). Zirconium and niobium oxides such as pyrochlore, monazite, armstrongite, mongolite and gittincite were described from pegmatites that are in II-W e.g., [36,62–64].

Andesite roof pendents are blackish and abundant plagioclase phenocrysts (Figure 4h). In the images of all spectral bands they are dark brown and determined age is yeilded of 330 Ma. e.g.,[30].

 doi:10.20944/preprints202401.1242.v1

Figure 4. Outcrop and hand specimen photos of alkali granites in eastern body and outcrop of dike and pegmatites. (a)- covered pendants fragments red colored I-E granite intruded into I-W, (b)- relationship between I-E and II-E, granite II-E intrude into I-E, (c)- hand specimen of the porphyry texture red granite , (d)- hand specimen of lilac granite, (e)- comendite dike outcrop intruding III-W granite, (f)- pantellerite lava lying in granite II-M, (g)- ekerite composition sheet pegmatites in intrusion I-M, (h)- outcrop of andesite roof pendant.

 doi:10.20944/preprints202401.1242.v1

4. Petrographical studies of the alkali granites

The average modal mineralogy of these granites is 65-70% K-feldspar (microcline), 25-28% quartz, 4-5% albite, and 7-9% aegirine and arfvedsonite or ferro-edenite. However, there is much variation in the relative abundances of ferromagnesian minerals. The pale pink color of granites from intrusion I-W and II-W is due to meso-perthitic albite stripes in K-feldspar. Aegirine and arfvedsonite have an agpaitic texture, and arfvedsonite replaces aegirine (Figures 5a and 5b). The darker red color that distinguishes the III-W granites is associated with the alteration of K-feldspar into pelitic aggregates *(Figures 5c and 5d).* The aegirine from granites of the western body has a pleochroic color from dark green to dark brown (Figure5c).

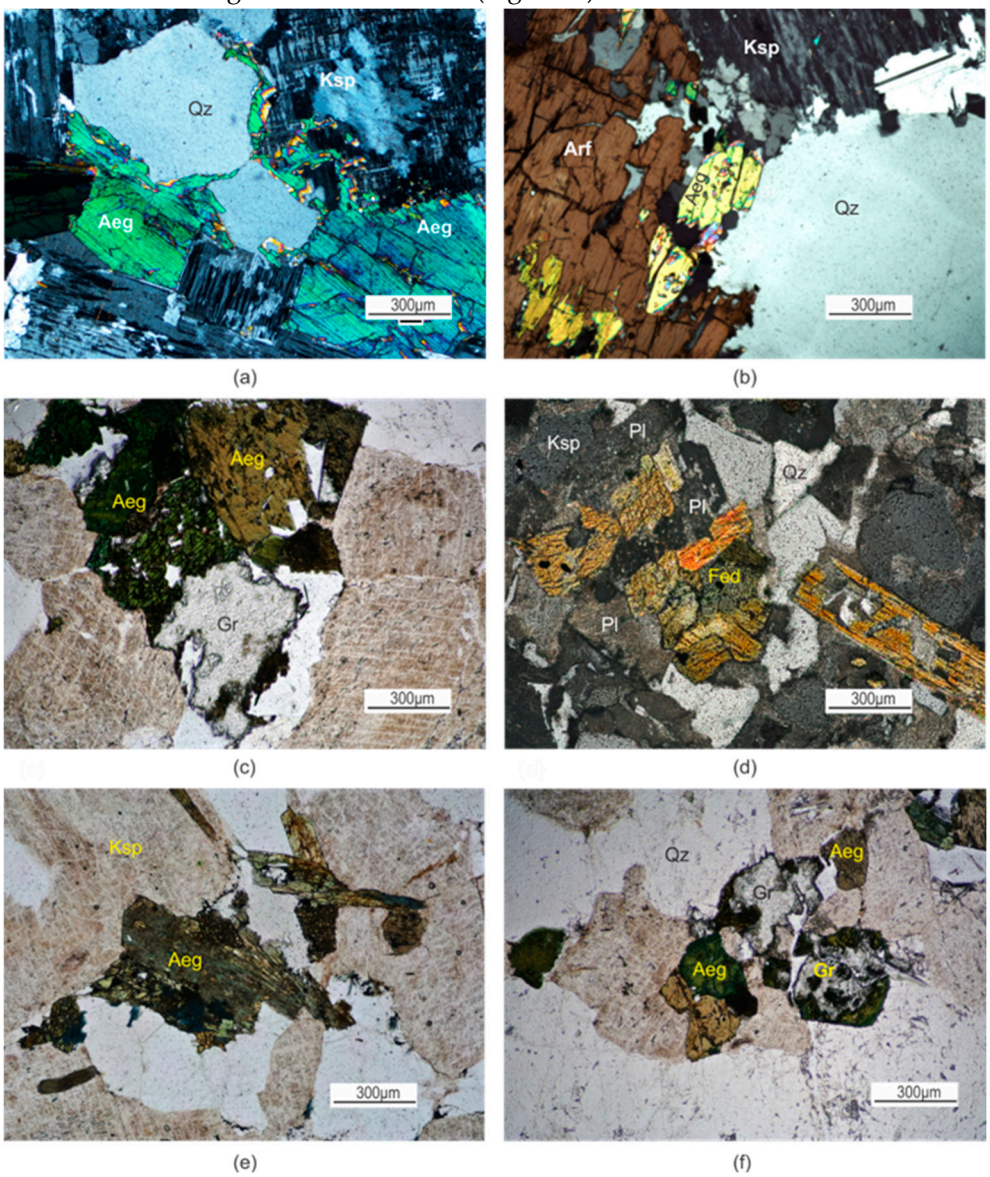

Figure 5. (a,b)- agpaitic texture of aegirine (Aeg)and arfvedsonite (Arf), and K-feldspar (Ksp) in the I-W and II-W units, (c)- aegirine (Aeg) and garnet (Gr) in quartz and K-feldspar (Ksp) ground mass, unit III-W, (d)- ferro-edinite (Fed), plagioclase (Pl)and K-feldspar (Ksp) phenocrysts in groundmass, consists of K-feldspar and quartz, (e)- fibrous aegirine (Aeg) crystals from granite in I-E unit, (f)-aegirine garnet and K-feldspar phenocrysts in I-E unit. (Mineral abbreviations are from [66].

Garnet is identified in accumulations of aegirine and arfvedsonite, and is eroded by them. This association is often described from granites III-M (Figure5c) than for granites I -M and II-M. Porphyritic red granite IV-W has cryptoperthitic K-feldspar, plagioclase and ferro-edenite and rare garnet e.g.,[49] that occur as a phenocryst and in the groundmass (Figure5d). Intrusions of the eastern

 doi:10.20944/preprints202401.1242.v1

body consist of porphyritic and equigranular granites. The proportion of ferrous minerals is less than in the granites of the western body. Fibrous to radiating or stellate acicular aegirine is predominant for the granites I-E. The aegirine pleochroic color of this intrusion illustrates a bluish tint among dark green and dark brown, in contrast to the western body (Figures 5e, 5f). Small (< 0.05 mm) garnet crystals are more conspicuous and are distinctive of intrusion II-E (Figure 5e).

5. Geochemistry of the Khanbogd alkali granites

Chemical analysis of oxides and calculated CIPW norms of the granites are listed in Table 1. Regardless of the presence of ferro-edenite, all granites plot as alkaline granites in TAS and AQPF diagrams [49]. The granites of all interpreted intrusions differ by the *aluminum saturation* index (ASI) by Shand e.g.,[50]. Granites of intrusions I-W, II-W and II-E are peralkaline. Granites of III-W show peraluminous affinity, the granites I-E vary from metaluminous to peraluminous. Hence, ferro-edenite granites are plotted in the metaluminous granite field excluding one data point (Figure 6a). Figures 6b-6f show a correlation between oxides and differentiation index (D.I). The silica content in granites of all intrusion is in the range of 71.00-78.36% (Table 1 and Figure 6a). The granites of the eastern body are characterized by high D.I. and this differs from the granites of the western body. Ferro-edinite granites differ in their content of SiO_2, CaO, MgO, K_2O from aegirine-arfvedsonite granites (Table 1, Figures 6b-6f). FeO variations indicate that the aegirine-arfvedsonite content in the granites of the eastern body is less than in the granites of the western body. Accordingly, they (I-E and II-E) are characterized by low Na2O, K2O and Fet contents compared to the granites of the western body (Figures 6b-6f). The studied granites also differ well in their CIPW norm calculated using the Hollocher program [21]. Granites I-M and II-M are acmite-Na-silicate (acm-ns) normative, with the exception small amount of ferrosilite (fs) and enstatite (en) molecules. Ilmenite is in norm, from these granites (Figure 6g). The anorthite- hypersthene (an-hy) molecule is calculated from aegirine-arfvedsonite granite III-M, and an-di-hy norm is acquired from ferro-edenite granites (Figure 6g). The granites of eastern body are peralkaline and metaluminous-peraluminous according to ASI. Acmit is calculated from (I-E), which is peralkaline, an-fs-en norm is calculated from II-E, which exhibit a metaluminous-peraluminous character. (Figure 6g, Table 1). Aegirine-arfvedsonite granites, in which a reduced amount of color minerals acquires a metaluminous and peraluminous character. The norm of ilmenite (il) of the I-W and II-W granites imply that they derived from a more reduced environment than others, for which near-neutral environment predominated (Figure6g). According to the K_2O/Na_2O ratio, all granites are rich in potassium; ekerite and pantellerite dikes are rich in Na (Table 1).

Table 1. Chemical composition and CIPW norms of alkali granites, Khanbogd pluton.

Samp.	32	35	37	39	41	21	30	31	48	72	51	52	54	18	19	61	62
№	I-W	I-W	I-W	I-W	I-W	II-W	II-W	II-W	II-W	II-W	III-W	III-W	III-W	IV-W	IV-W	IV-W	IV-W
SiO_2	75.68	73.12	75.13	74.41	74.48	76.08	73.21	75.76	72.54	73.01	75.04	74.45	74.15	71.94	71.18	71.00	71.46
TiO_2	0.21	0.21	0.27	0.30	0.18	0.23	0.30	0.21	0.42	0.37	0.23	0.21	0.36	0.41	0.40	0.49	0.38
Al_2O_3	10.90	11.24	10.51	11.06	10.63	10.81	11.65	10.35	11.89	11.19	11.88	12.12	12.30	13.22	13.79	13.63	13.49
Fe_2O_3	0.50	0.69	0.58	0.56	0.57	0.49	0.56	0.56	0.60	0.65	0.37	0.41	0.54	0.47	0.40	0.40	0.41
FeO	3.37	4.59	3.86	3.76	3.80	3.26	3.74	3.73	4.03	4.35	3.45	3.34	3.38	3.14	2.65	3.38	2.76
MnO	0.10	0.08	0.12	0.06	0.11	0.12	0.16	0.10	0.16	0.18	0.10	0.12	0.01	0.04	0.11	0.04	0.11
MgO	0.12	0.18	0.13	0.12	0.07	0.12	0.23	0.10	0.37	0.25	0.18	0.22	0.13	0.44	0.43	0.48	0.41
CaO	0.14	0.24	0.28	0.29	0.15	0.21	0.40	0.22	0.75	0.18	0.16	0.27	0.15	1.03	1.03	1.11	1.11
Na_2O	4.08	4.58	4.22	4.41	4.52	3.69	4.52	4.08	4.46	4.68	3.75	3.71	3.80	4.31	3.86	4.12	4.23
K_2O	4.65	4.93	4.76	4.79	4.84	4.73	5.05	4.41	4.75	4.81	4.79	4.96	4.96	5.07	5.53	5.21	5.23
P_2O_5	0.00	0.01	0.00	0.06	0.01	0.00	0.02	0.00	0.05	0.03	0.01	0.05	0.04	0.08	0.08	0.10	0.07
ppm	0.35	0.27	0.20	0.37	0.69	0.38	0.27	0.65	0.14	0.48	0.26	0.30	0.23	0.14	0.45	0.31	0.53
Total	100.1	100.1	100.1	100.1	100.0	100.1	100.1	100.1	100.1	100.0	100.2	100.1	100.1	100.2	99.91	100.1	100.1
ASI	0.91	0.84	0.93	0.85	0.87	0.93	0.86	0.87	0.86	0.85	1.02	1.01	1.03	0.92	0.97	0.98	1.01
D.I	90.66	86.88	88.45	89.00	87.98	91.79	88.51	89.18	87.75	86.87	91.69	91.24	91.67	89.55	88.56	87.69	89.37
Fet	3.87	5.28	4.44	4.32	4.37	3.75	4.30	4.29	4.63	5.0	3.82	3.75	3.92	3.61	3.05	3.78	3.17
K/N	1.14	1.08	1.13	1.09	1.07	1.28	1.12	1.08	1.07	1.03	1.28	1.34	1.31	1.18	1.43	1.24	1.24
CIPW																	
Q	33.01	27.39	32.77	30.49	31.66	34.03	26.87	34.44	25.00	27.97	31.66	30.54	30.22	23.27	23.22	22.57	22.67

 doi:10.20944/preprints202401.1242.v1

Or	27.48	29.13	28.13	28.30	28.60	27.95	29.84	26.06	28.06	28.42	28.30	29.31	29.31	29.96	32.68	30.26	30.91
Ab	30.17	30.36	27.55	30.21	27.72	29.26	31.80	26.68	34.69	30.26	31.73	31.39	32.15	36.32	32.66	34.86	35.79
An	0.00	0.00	0.00	0.00	0.00	0.00	0.00	0.00	0.00	0.00	0.73	1.01	0.48	1.74	3.96	3.57	2.37
C	0.00	0.00	0.00	0.00	0.00	0.00	0.00	0.00	0.00	0.00	0.26	0.28	0.50	0.00	0.00	0.00	0.00
Ac	1.45	2.00	1.68	1.62	1.65	1.42	1.62	1.62	1.74	1.88	0.00	0.00	0.00	0.00	0.00	0.00	0.00
Ns	0.63	1.43	1.45	1.22	2.01	0.08	1.07	0.93	0.25	1.67	0.00	0.00	0.00	0.00	0.00	0.00	0.00
Di(wol	0.00	0.00	0.00	0.00	0.00	0.00	0.00	0.00	0.00	0.00	0.00	0.00	0.00	0.00	0.00	0.00	0.00
Di (en)	0.28	0.42	0.30	0.28	0.17	0.27	0.51	0.23	0.74	0.60	0.45	0.55	0.32	0.86	1.01	1.09	0.79
Di (fs)	5.72	7.73	6.24	6.05	6.57	5.37	5.88	6.19	5.63	7.41	5.86	5.67	5.37	3.74	3.86	4.68	3.34
Hy (fs)	0.58	0.93	1.17	0.88	0.59	0.87	1.49	0.93	2.58	0.56	0.00	0.00	0.00	1.94	0.41	0.88	1.82
Hy en)	0.03	0.06	0.06	0.05	0.02	0.05	0.15	0.04	0.39	0.05	0.00	0.00	0.00	0.51	0.12	0.23	0.50
Mt	0.00	0.00	0.00	0.00	0.00	0.00	0.00	0.00	0.00	0.00	0.54	0.59	0.78	0.68	0.58	0.58	0.59
Il	0.40	0.40	0.51	0.57	0.34	0.44	0.57	0.40	0.80	0.70	0.43	0.40	0.68	0.78	0.76	0.93	0.72
Ap	0.00	0.03	0.00	0.14	0.03	0.09	0.05	0.05	0.12	0.08	0.02	0.13	0.09	0.20	0.20	0.25	0.17
samp.	**4**	**9**	**11**	**12**	**1**	**2**	**3**	**8**	**33**	**34**	**69**	**64**	**73**	**55**	**13**		
№	**I-E**	**I-E**	**I-E**	**I-E**	**II-E**	**II-E**	**II-E**	**II-E**	**eker.**	**eker.**	**eker.**	**pant.**	**pant.**	**com.**	**com.**		
SiO_2	78.36	78.09	77.46	77.34	76.04	76.08	75.91	75.81	73.58	73.35	73.39	76.50	73.00	77.11	76.78		
TiO_2	0.22	0.11	0.11	0.12	0.21	0.21	0.22	0.24	0.36	0.21	0.22	0.23	0.23	0.10	0.27		
Al_2O_3	10.97	11.30	11.37	11.44	11.40	11.23	11.55	11.65	11.05	9.05	9.44	10.89	9.24	11.67	10.60		
Fe_2O_3	0.39	0.26	0.27	0.25	0.38	0.42	0.38	0.36	0.30	0.37	0.98	0.47	1.03	0.54	0.50		
FeO	2.57	1.71	1.81	1.66	2.55	2.78	2.55	2.38	3.86	6.40	6.51	3.14	6.85	0.88	3.32		
MnO	0.09	0.06	0.06	0.04	0.10	0.11	0.10	0.11	0.17	0.20	0.20	0.10	0.27	0.13	0.06		
MgO	0.12	0.12	0.12	0.12	0.12	0.13	0.13	0.12	0.25	0.06	0.10	0.09	0.15	0.42	0.11		
CaO	0.37	0.20	0.27	0.30	0.20	0.22	0.14	0.32	0.55	0.14	0.16	0.17	0.17	0.27	0.59		
Na_2O	3.46	3.64	3.76	3.52	3.91	3.81	3.96	3.98	4.67	4.78	4.52	4.28	4.68	4.17	3.10		
K_2O	4.44	4.33	4.42	4.57	4.66	4.61	4.75	4.75	4.43	4.14	4.12	3.86	4.29	5.39	4.60		
P_2O_5	0.01	0.00	0.00	0.00	0.00	0.00	0.00	0.00	0.05	0.02	0.00	0.00	0.00	0.01	0.00		
ppm	0.38	0.41	0.51	0.67	0.54	0.47	0.50	0.41	0.74	0.27	0.40	0.44	0.24	0.37	0.57		
Total	100.3	100.2	100.1	100.0	100.1	100.0	100.1	100.1	100.0	100.1	100.1	100.1	100.1	101.0	100.1		
ASI	0.96	0.96	0.97	0.95	0.98	1.02	0.99	1.01	0.82	0.88	0.74	0.94	0.73	0.89	0.97		
D.I	93.01	94.82	94.51	94.10	93.43	93.09	93.54	93.01	87.67	81.26	86.53	91.78	80.16	93.13	90.80		
Fet	2.96	1.97	2.08	1.91	2.93	3.20	2.93	2.74	4.16	5.77	6.04	3.61	7.88	1.42	3.72		
K/Na	1.28	1.19	1.18	1.30	1.19	1.21	1.20	1.19	0.95	0.87	0.91	0.90	0.92	1.29	1.48		
CIPW																	
Q	37.49	38.44	36.59	37.32	33.20	33.76	32.51	32.22	29.34	28.07	28.54	34.45	31.18	32.27	37.39		
Or	26.24	25.58	26.11	27.00	27.54	27.24	28.07	28.07	26.17	24.46	24.35	22.81	25.35	31.85	27.18		
Ab	29.28	30.80	31.81	29.78	32.69	32.09	32.96	33.47	32.17	33.78	33.64	34.52	23.63	30.01	26.23		
An	1.28	0.99	1.10	1.49	0.00	0.00	0.00	0.00	0.00	0.00	0.00	0.00	0.00	0.00	1.42		
C	0.00	0.26	0.00	0.16	0.00	0.00	0.00	0.00	0.00	0.00	0.00	0.00	0.00	0.00	0.00		
Ac	0.00	0.00	0.00	0.00	0.35	0.13	0.48	0.18	0.86	1.07	0.87	1.36	2.98	1.56	0.00		
Ns	0.00	0.00	0.00	0.00	0.00	0.00	0.00	0.00	1.48	1.27	0.84	0.04	2.93	0.81	0.00		
Di(wol	0.00	0.00	0.00	0.00	0.00	0.00	0.00	0.00	0.00	0.00	0.00	0.00	0.00	0.00	0.00		
Di (en)	0.28	0.03	0.30	0.30	0.27	0.29	0.30	0.25	0.50	0.63	0.24	0.21	0.36	0.84	0.24		
Di (fs)	4.00	2.86	2.92	2.72	3.88	4.18	4.03	3.25	5.79	9.69	10.24	5.25	12.37	1.36	4.50		
Hy (fs)	0.40	0.00	0.20	0.00	0.81	0.89	0.56	1.29	1.91	0.46	0.57	0.60	0.61	0.63	1.26		
Hy en)	0.03	0.00	0.02	0.00	0.07	0.07	0.05	0.11	0.20	0.03	0.02	0.03	0.02	0.44	0.08		
Mt	0.56	0.38	0.39	0.36	0.38	0.54	0.31	0.43	0.00	0.00	0.00	0.00	0.00	0.00	0.73		
Il	0.42	0.21	0.21	0.23	0.40	0.40	0.42	0.46	0.68	0.40	0.42	0.44	0.44	0.19	0.51		
Ap	0.02	0.00	0.00	0.00	0.00	0.00	0.00	0.00	0.12	0.01	0.00	0.00	0.00	0.02	0.00		

eker.- ekerite, pant.- pantellerite, com-comendite dikes.

 doi:10.20944/preprints202401.1242.v1

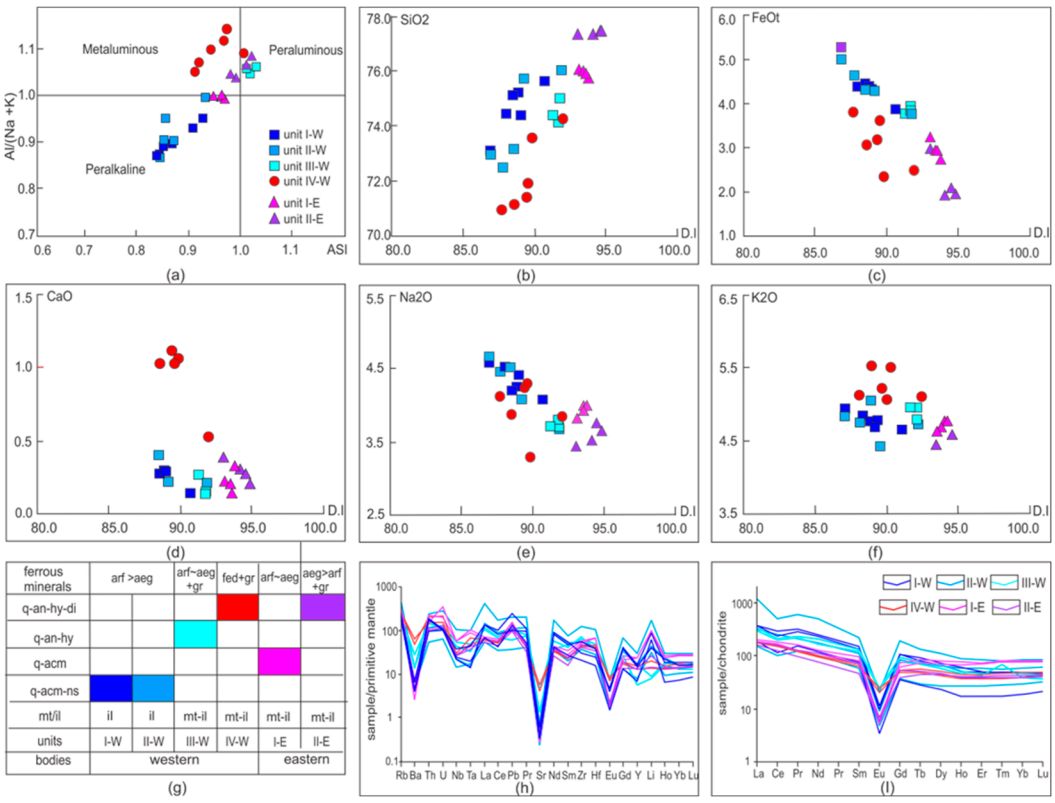

Figure 6. Correlation diagrams. (a)- granites plot in ASI diagram [50], (b-f) major oxides vs D.I. diagrams, (g)- calculated norms from alkali granites in different intrusions, (h)- primitive mantle normalized patterns of multi-element data of alkali granites, (i)- chondrite-normalized REE patterns of alkali granites of different intrusions, normalized values are from [54].

The trace and REE analysis of the granites are shown in Table 2. The Li content is in 32-68 ppm for I-W units and 6-15 ppm for units IV-W. Some samples contain high Zr content associated with the mineralization of zirconium oxides, such as elpidite (Table 2). In the trace element distribution diagram normalized to the primitive mantle, deep negative anomalies of Ba, Sr, Eu and positive anomalies of Th, U, Pb, Li are observed (Figure 6h). A pattern with more deep negative anomalies of Ba and Sr is revealed in granites II-E and II-W. Although, less pronounced negative anomalies of Ba, Sr and Eu are marked from ferro-edenite granites (Figure 6h). The chondrite-normalized REE patterns from granites are sub-symmetric, with Eu deep negative anomalies (Figure 6i). In this diagram, the ferro-edenite granite pattern is intermediate between pattern of others, and their Eu anomalies are at a higher level than the others (Figure 6i).

Table 2. Trace and REE analysis of alkali granites, Khanbogd alkali granite pluton.

Sam	32	35	37	39	41	21	30	31	48	72	51	52	54	18	19	61	62
№	I-W	I-W	I-W	I-W	I-W	II-W	II-W	II-W	II-W	II-W	III-W	III-W	III-W	IV-W	IV-W	IV-W	IV-W
Ba	30.27	49.51	52.59	28.83	9.79	33.64	106.09	18.10	159.20	96.14	98.63	125.16	196.47	348.37	473.03	441.00	389.84
Be'	6.75	7.65	5.27	4.40	3.55	3.77	4.16	6.98	5.25	13.34	4.37	6.25	7.14	6.54	5.66	4.63	8.52
Cr	3.66	3.28	3.24	3.87	3.91	2.60	5.57	1.80	0.93	1.63	2.06	5.68	2.46	1.23	5.23	3.74	2.06
Ga	29.64	29.02	29.14	28.07	29.99	26.37	23.41	26.95	25.53	26.47	22.16	14.26	25.29	23.65	20.91	22.55	22.18
Hf '	5.04	8.11	10.52	12.43	93.20	8.75	14.57	17.43	19.24	31.89	11.46	17.82	15.18	13.91	14.12	12.45	31.87
Li'	48.27	68.22	62.37	31.75	71.02	23.26	80.43	76.19	47.95	128.30	5.85	5.54	6.52	14.97	12.42	9.98	100.18
Nb'	18.18	28.63	72.86	16.13	221.41	10.55	75.66	36.42	24.24	75.36	37.66	28.01	30.78	20.66	23.42	18.97	26.24
Ni	1.17	1.39	4.60	1.48	1.73	1.75	3.98	1.64	4.77	4.26	1.05	1.11	4.71	4.33	1.41	2.92	3.31
Pb	26.33	47.07	43.88	20.51	16.40	6.77	36.33	21.32	8.59	37.33	11.05	9.04	19.60	28.60	24.51	21.60	21.69
Rb*	157.96*	172.04*	250.29	130.92*	161.46*	123.30*	250.41*	155.90	135.41*	286.71*	138.50	101.5*	144.77*	159.92*	179.73*	159.71*	161.70*
Sr*	7.06*	13.83*	15	7.61*	6.13*	7.32*	27.92*	7.50	33.73*	15.40*	15.06	30.60*	28.89*	87.18*	105.94*	117.4*	9.06*
Ta'	0.86	1.93	1.04	0.62	7.74	0.71	1.22	1.30	2.01	4.03	1.96	1.82	1.38	2.76	1.54	2.03	1.33
Th'	16.21	16.90	20.16	8.48	14.54	4.63	36.33	6.41	13.89	19.82	9.81	7.77	12.63	16.84	20.39	13.23	9.61

 doi:10.20944/preprints202401.1242.v1

U'	2.26	2.37	2.51	2.25	3.58	1.34	3.32	3.91	3.77	6.03	2.72	4.30	2.41	4.54	4.00	3.25	3.51
V	2.85	0.77	4.25	1.99	4.87	48.01	0.98	5.99	23.12	15.40	6.97	7.58	23.92	24.77	13.53	29.82	23.97
Y	32.76	81.01	206.46	73.24	57.81	36.81	192.42	80.84	91.55	137.10	26.63	37.64	76.80	69.16	52.29	58.60	55.62
Zr	240.33	359.79	2277.83	648.43	3459.1	422.63	1812.2	1346.6	767.22	1383.9	782.10	389.03	709.58	519.71	414.66	479.03	414.10
La	50.26	98.20	95.26	100.00	73.44	37.06		74.20	64.32	278.80		71.65	81.27	42.14	42.07		35.65
Ce	79.85	196.00	150.72	153.50	141.50	63.29		152.63	152.26	304.50		122.14	127.63	96.54	92.07		82.11
Pr	15.77	32.53	16.37	28.29	18.22	11.39		19.89	18.91	57.15		21.03	21.84	12.01	11.58		10.03
Nd	61.87	130.80	98.53	116.30	71.33	119.09		82.54	76.57	232.90		79.23	97.76	48.23	45.22		39.23
Sm	13.07	25.94	15.65	22.44	12.91	25.44		17.12	16.18	34.27		18.52	20.38	10.77	9.81		8.52
Eu	0.26	0.82	0.71	0.70	0.41	0.28		0.53	0.97	1.25		1.38	1.41	1.21	1.42		1.22
Gd	8.44	24.67	15.76	23.92	12.46	7.67		17.52	16.36	40.40		15.99	19.38	11.23	10.22		8.99
Tb	1.20	3.49	2.91	3.75	1.79	1.12		2.68	2.95	4.99		2.62	2.89	2.08	1.80		1.64
Dy	6.77	19.71	15.38	20.09	10.80	6.94		16.29	17.82	28.36		15.22	17.30	12.93	11.07		10.22
Ho	1.15	3.29	1.93	3.82	2.19	1.51		3.31	3.42	4.91		2.63	2.97	2.55	2.10		2.04
Er	3.39	9.67	8.25	9.49	6.32	4.51		9.65	10.08	13.77		7.12	7.92	7.45	6.24		5.95
Tm	0.52	1.42	1.36	1.46	0.95	0.71		1.42	1.54	2.02		1.96	1.17	1.20	0.97		0.96
Yb	3.90	9.75	12.47	9.11	6.52	5.10		9.92	10.62	14.39		6.52	7.93	8.23	6.67		6.52
Lu	0.66	1.44	1.36	1.34	1.05	0.82		1.59	1.61	2.18		0.94	1.12	1.22	1.12		0.95

Sam№	**4 I-E**	**9 I-E**	**11 I-E**	**12 I-E**	**1 II-E**	**2 II-E**	**3 II-E**	**8 II-E**	**33 eker.**	**34 eker.**	**69 eker.**	**64 pant.**	**73 pant.**	**55 com.**	**13 com.**
Ba.	57.73	33.46	18.77	45.52	29.28	52.40	53.78	31.71	99.71	23.1	30.12	30.35	59.93	57.36	13.48
Be'	6.59	7.51	6.59	9.31	4.17	4.85	5.00	4.12	8.07	8.45	6.56	4.36	9.14	5.84	7.26
Cr	0.52	0.71	1.70	2.68	1.46	1.82	3.85	0.06	0.8	0.8	0.57	1.33	6.03	0.77	2.84
Ga	23.03	24.02	24.79	24.06	23.80	23.39	23.46	23.46	40.54	51.74	34.51	41.12	29.18	7.39	26.11
Hf '	19.53	20.80	20.58	19.76	10.15	9.74	12.32	11.05	26.42	31.87	21.52	31.87	41.02	12.55	18.24
Li'	58.66	70.01	74.24	51.05	21.05	16.77	19.40	10.99	47.0	99.23	84.51	100.18	102.96	63.27	48.43
Nb'	30.35	41.19	41.49	44.63	25.92	44.07	20.47	18.79	35.97	23.64	9.89	23.64	61.10	9.02	39.35
Ni	2.28	3.80	4.55	4.37	1.39	3.82	3.32	2.92	2.45	1.31	1.86	2.16	7.02	0.71	3.87
Pb	25.05	29.06	18.60	48.43	25.60	45.25	18.14	21.60	42.14	17.96	2.40	17.96	12.23	5.50	25.69
Rb*	147.71	231.45*	256.42*	242.90*	127.32	170.42	140.89*	116.31*	143.59	160.96*	261.05*	149.4*	446.2*	144.66*	148.47*
Sr*	10.10	6.48*	5.8*	11*	5.84	8.29	10*	8*	36.40	6.56*	4.08*	4.69*	16.33*	11.79*	11.12*
Ta'	4.54	3.61	4.30	3.74	1.03	2.17	1.80	1.51	2.37	1.33	1.52	1.43	2.37	1.73	3.17
Th'	10.38	19.56	13.29	20.06	7.48	18.26	9.51	8.45	21.26	13.15	2.86	8.64	9.25	3.80	10.74
U'	2.12	4.28	7.28	6.00	2.11	1.85	2.80	2.42	5.79	3.51	4.66	3.05	7.52	3.10	2.85
V	2.39	0.00	2.75	4.15	2.29	2.21	5.64	1.62	1.25	2.54	0.96	1.04	1.12	0.93	1.76
Y	74.40	108.68	108.30	129.40	62.17	109.40	61.50	59.77	135.23	107.08	12.10	130.29	249.03	19.93	93.34
Zr	627.82	576.45	655.40	614.72	524.12	1096.7	539.50	463.52	1075.9	1456.6	487.30	717.26	3383.1	178.02	1155.4
La		43.39	48.82	48.39			38.26	43.95	107.28	18.64			148.13	40.51	
Ce		102.73	112.85	104.73			80.32	101.10	235.62	57.52			157.40	92.05	
Pr		12.54	15.17	13.97			9.28	12.22	30.40	5.64			25.78	12.59	
Nd		51.85	60.66	57.79			36.77	53.48	128.53	25.48			80.33	52.45	
Sm		12.75	15.21	14.76			7.38	10.80	26.50	9.28			29.28	12.36	
Eu		0.31	0.36	0.41			0.33	0.40	1.13	0.37			10.38	1.50	
Gd		12.82	15.75	15.44			8.24	11.22	27.51	13.83			24.83	11.24	
Tb		2.83	3.23	3.36			1.68	1.95	4.23	2.77			2.58	1.52	
Dy		18.40	20.92	21.74			11.41	11.96	26.75	19.26			19.20	10.58	
Ho		3.91	4.37	4.38			2.35	2.23	5.44	4.15			4.15	2.32	
Er		11.89	12.62	13.35			6.91	6.50	16.07	12.53			13.53	7.10	
Tm		1.98	2.12	2.15			1.09	1.00	2.33	1.84			2.14	1.14	
Yb		13.30	14.25	14.23			7.22	6.85	15.43	12.62			14.55	7.82	
Lu		1.98	2.13	2.07			1.12	1.05	2.28	2.03			2.20	1.14	

Note: ' ICP-MS; * Isotope Dilution; it is marked in Sr and Rb.

5. Sr, Nd, Hf, Pb and O isotopes of the alkali granites Khanbogd pluton

The initial of $^{87}Sr/^{86}Sr$ and $^{143}Nd/^{144}Nd$ were calculated for samples on Rb-Sr whole rock isochron age of 295.7 Ma, and the Sr isotope ratios were measured for most samples. The 295.7 Ma was obtained twice, first from all aegirine-arfvedsonite granites including ekerite and comendite dikes, and second from granites I-M, II-M and III-M (Supplementary Table S1) e.g.,[49]. According to this measurement, $^{87}Sr/^{86}Sri$ values range from 0.6676 to 0.7077 for the aegirine-arfvedsonite granites, except for one value of 0.7287. $^{143}Nd/^{144}Ndi$ values of the granites are moderately high, from 0.5125 to 0.5127. A slightly higher initial $^{87}Sr/^{86}Sr$ of 0.7051-0.7071 was obtained from ferro-edenite granites

 doi:10.20944/preprints202401.1242.v1

with their isolated plots of 269.6 ± 2.8 Ma (Supplementary Table S1). Also 291±7.2 Ma was detected from aegirine-arfvedsonite granites of two bodies, excluding dikes (Supplementary Table S1).

The received ages of 291±7.2 and 295.7±5.3 Ma are not only consistent with the geological relationship, but also with U/Pb zircon dating by Kovalenko et al. [30]. These are 290±1 Ma from coarse grained granite and 292±1 Ma for a pegmatite I-M. All εNdt values are positive in the range 6.20-7.80 for aegirine-arfvedsonite granites, 3.95-5.99 for ferro-edenite granites, and 5.06-6.98 for dikes (Supplementary Table S2). The positive and moderate values of Ndi suggest that the alkali granites were derived from a modified mantle source. This is approved by the plots of the alkali granites in diagrams of T-εNd (t), Pb^{207}/Pb^{204}-Pb^{206}/Pb^{204}, εNd(t) -εHf (t) and Sri-δ18O‰ (Figure 7a-7c), e.g.,[49]. Source definition for CAOB granites by the ratio of T and εNd was first proposed by Hong et al. [22]. Here, in this manuscript, the CAOB field constructed by Serjlkhumbe [49] is used, which was supplemented by data from Kovalenko et al. [31] and e.g., [20,49]. In this diagram, the granites of the Khanbogd pluton are located closer to the line indicating mantle origin than the granites of the Hercynite Belt of Mongolia (Figure 7a). The Pb^{207}/Pb^{204} - Pb^{206}/Pb^{204} system also shows a melt source from mantle-derived rocks e.g., [71] for the Khanbogd granites (Figure 7b). In the εHf (t) vs. εNd (t) diagram, the values of the Khanbogd granites are plotted near the depleted mantle line [60]. The measured $\delta^{18}O$‰ data from quartz are in range of 6.67-9.2‰ for the granites of western body (Table 3). Low $\delta^{18}O$‰qz values are characteristic of granites I-E, and granites II-E are specified by low $^{87}Sr/^{86}Sr$ content, while the δ18O‰qz values are same as for III-W and IV-W (Table 3, Figure 7b). Most of the plots in Sri-δ18O‰ diagram demonstrate oxygen that has dilated from mantle derived rocks (Figure 7d).

Table 3. $^{87}Sr/^{86}Sri$ at 291 Ma and $\delta^{18}Oqz$‰ data of alkali granites, Khanbogd pluton.

sample	32	35	39	21	30	72	52	54	18	19	09	11	03	08	55	34
№	I-M	I-M	I-M	II-M	II-M	II-M	III-M	III-M	IV-M	IV-M	I-E	I-E	II-E	II-E	com.	eke.
$^{87}Sr/^{86}Sr_{291}$	0.7017	0.7077	0.7049	0.7079	0.6982	0.7049	0.7012	0.7029	0.7035	0.7056	0.6753	0.6945	0.7065	0.7056	0.7026	0.6944
$\delta^{18}Oqz$ ‰	8.17	8.11	7.29	7.06	6.67	7.18	8.4	9.52	8.34	9.20	8.71	9.05	4.92	5.72	8.33	6.97

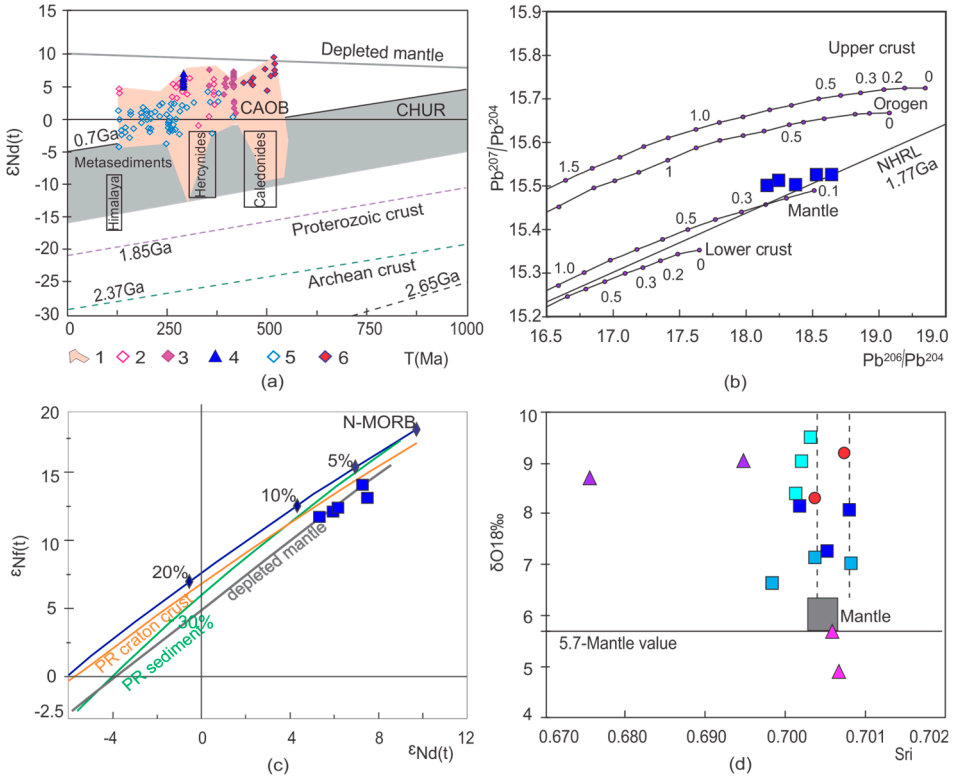

Figure 7. Isotope plots. (a)- Intrusive ages vs. εNd (t) diagram. 1-CAOB field is done by data of Mongolian granites [49] used the field of [22], 2-4 granites data of Hercynide belt of Mongolia: 2- by

 doi:10.20944/preprints202401.1242.v1

Kovalenko et al. [31], 3- by Helo et al. [20], 4-Khanbogd granites by Serjlkhumbe [49], 5- granites data of Caledonian belt of Mongolia, Kovalenko et al. [31], 6-granites of Zavhan microcontinent [31]. Fields of Caledonides, Hercynides and Himalaya - from Patchett [43], metasediments data from [31]. (b)-Khanbogd granite plots in Pb isotopic systematics [48] upper, and lower crust, orogen and mantle evolution curve by [71], Tick marks represent 0.1 Ga age intervals. (c)- Khanbogd granite plots in εHf (t) vs. εNd(t) diagram [49], N-MORB [41], Proterozoic continental crust [61], Proterozoic sediment data and mantle arrow are from [60], (d)-granite plots in $^{87}Sr/^{86}Sr$ - $\delta^{18}Oqz$ diagram. The dotted lines are approximate ranges of $^{87}Sr/^{86}Sri$ - $\delta^{18}Oqz$ in mantle derived rocks [39].

6. Discusstion

The most cited source models for alkaline granites have been based on their low $^{87}Sr/^{86}Sr$ ratio, which is similar to depleted and modified mantle origin. Models for their genesis include: (1) fractionation of mantle-derived magmas with or without interaction of crustal rocks [11,15,37]; (2) partial melting production of residue from type-I granites [5]; (3) crustal melting accompanied by an influx of mantle fluids [19]; (4) partial melting of metasomatically altered crustal source rocks [3,65]; and (5) partial melting of lower crustal basalt and lithospheric mantle induced by a rising plume [9,10]. The vapor absent melting from mica schist, tonalite and biotite-amphibole gneiss model [7.53, 44] differed from the aforementioned models. For the Khanbogd pluton complex, its origin has been attributed to hypothesis (1) that was proposed by Vladykin et al. [63]. Kovalenko et al. [29.30] proposed a magma source originating from the melt that resulted from the interactions of enriched mantle, depleted mantle, and crust materials. With the exception of low $^{87}Sr/^{86}Sri$ values, the trace elements content such as Th, Ta, Nb, La and Yb of studied granites is identical to the content of mafic rocks, which having melt sources from the lithospheric and asthenospheric mantle [1 and 45]. In the $^{87}Sr/^{86}Sr$-$\delta^{18}O$ correlation diagram, the samples illustrate plots in 3 directions: Precambrian gneisses, seafloor deposits, and depleted mantle (Figure 8a). Ocean-floor sediments are considered a resource of Rare Earth Elements e.g. Kato et al. [26], Yasukawa et al. [69], Takaya et al. [55], Milinovic et al. [40]. Therefore, the REE concentration in the alkaline granites of Khanbogd pluton does not negate the participation of modified ocean floor rocks in their magmatic source. As for the melting of tonalites and granite-gneisses into a magma source for alkaline granites, this has long been confirmed experimentally [7,18,44,53].

Moreover, Patino Douce [44] obtained the leucogranite composition from an experiment on tonalite in vapor absent melting at the 15-32 kbar. Several reactions have been illustrated as experimental results in a phase diagram [44]. One of the reactions is an association "Cpx + Grt + Kfsp + melt" from the melt "Bi + Am + Pl + Q". The diverse extent of garnets in thin sections indicates that this reaction was involved in the formation of alkaline granite of the studied pluton. Nevertheless, negative anomalies of Ba, Sr, Eu and positive anomalies of Th, U, Pb, Li in the studied granites indicate the presence of a vapor absent melt for their crystallization e.g., [18].

Petford [46] and Wilson et al. [67] suggest that the flattened intrusions and ring dikes are associated with magma at shallow depths, where the fluid absent melt is conditioned. On the other hand, the half ring dikes are accompanied by detachments of the thrust system [13,57]. Uplifted country rocks between the granite intrusions and pendants on the top of the granites suggest that the granites were penetrated along fractured country rocks. Except for the flattened shape, the two adjacent intrusive bodies and the undeformed Carboniferous volcanic rocks in the front part of the pluton are consistent with underplating magma factors during duplex-type thrusts, as discussed in the modeling of Konstantinovskaya and Malavieille [28], Malavieille [38]. As defined by Cox [6], the presence of basalt and rhyolites supports igneous underplating during continental basaltic volcanism. The studied alkali granite pluton is temporary coeval with Permian volcanic formation of basalt and comendite (rhyolite) e.g., [29–31]. As well as Thybo and Nielsen [58], have proposed that magma underplating also accompanies the rift zone. In our case, the role of underplating magma source is confirmed by variable $^{87}Sr/^{86}Sr_i$ and $\delta^{18}O$ values, demonstrating multiple melt sources for the alkali granites, as well as melt from mantle rocks, recycled rocks of continental and oceanic arcs (Figure 8a). The Figure 8b presents a model for the studied Khanbogd pluton.

 doi:10.20944/preprints202401.1242.v1

We expressed our interest to geophysicists of the "Geo-Oron" Company to study gravimetric models of another largest alkali-granite pluton, Bayan-Ulan, located in Central Mongolia. As a result of modeling, a flattened shape was obtained for this pluton [14], (Figure 8c). Bayan-Ulan pluton occupies almost 1000 sq.km and emplaced into accretionary wedge complex [2]. The detrital zircon age of this complex correlated to the interval of Permian-Triassic [4]. Granites of Bayan-Ulan pluton consist mainly of quartz, K-feldspar, aegirine, riebeckite and rarely biotite. They are associated with leucogranite [32]. The U/Pb zircon age of 221 Ma was determined from alkaline granite [10].

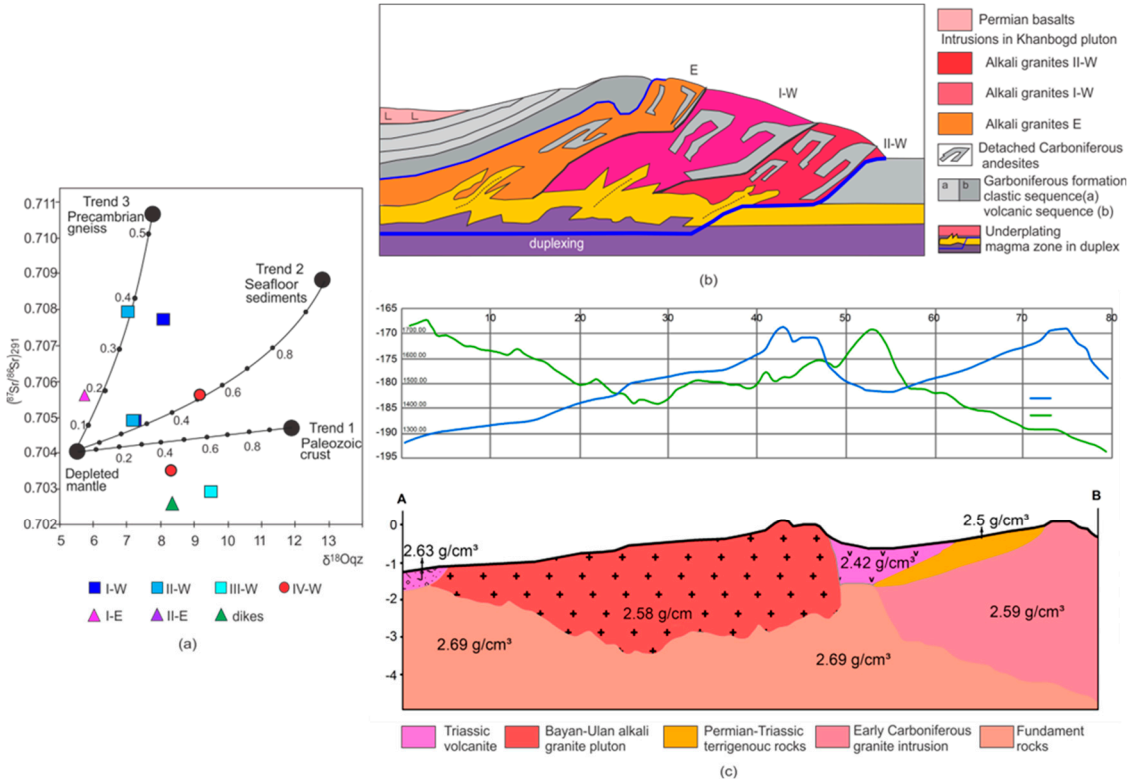

Figure 8. Model for Khanbogd pluton. (a)- plots in $^{87}Sr/^{86}Sr_{291}$ - $\delta^{18}Oqz$ diagram. Trend curves of terrigenous sediment from [42], sea floor sediment from [47] and depleted manle from Eiler et al. [12], (b)- suggested model for the emplacement of flattened form alkali granites Khanbogd pluton, (c)- gravimetric model for Bayan-Ulan alkali granite pluton.

The elliptical shape of the Bayan-Ulan alkaline granite complex among the accretionary complex implies a magma inflation along the thrust faults in accretionary zone. This assumption refutes the hypothesis that the underplating magma followed the rift zone. However, the geological setting of the Bayan-Ulan pluton shows that alkaline granites can also form where thrusting followed in the accretion zone, of course, not in all cases. The low isotope values, the thrust nature and 295–286 Ma ages of the alkali granites, indicate an underplate magma evidenced during Permian rifting.

Similar events, such as magma rising along horizontal faults and underplating magma source were suggested for the Permian alkaline granite plutons of China e.g., [59,72,73]. This shows that the Permian alkali granite plutons were evidenced by similar processes in southern Mongolia and northern China.

7. Conclusions

1. The peralkaline Khanbogd plutonic complex with an area over >1000sq.km formed by the sequential emplacement of several elliptic intrusions that were occurred along the sub horizontal fracture zones of duplex type of thrusting.
2. The geochemistry characteristic of alkaline granites with low Sr, Ba, Eu, Ti and high Th, U, Pb and Li shows a crystallization affinity from vapor absent melt due to fracture zones.
3. The low of Sr, Pb,Hf and O isotope values , as well as the thrust nature of the alkali granites, indicate an underplate magma source evidenced during duplexing of Permian period

4. The ratios of $^{87}Sr/^{86}Sr_i$ vs. $\delta^{18}O$ of alkali granites indicate their formation from an underplate melting, where mantle sourced rocks were involved

Supplementary Materials: The following supporting information can be downloaded at the website of this paper posted on Preprints.org.

Funding: This research received no external funding, however based on chemistry analyses, which was granted by the done by Master and Doctaral thesis of doc. AmarAmgalan Field geological studies of this large pluton, re-examined as part of the project "ACCRETIONAL OROGEN OF SOUTHERN MONGOLIA: A COMPARISON OF THE CENTRAL ASIAN OROGEN (CAOB) IN MONGOLIA AND CHINA - (NFSC2019/04).

Acknowledgmnts: We specially thanked to geologists Baatar Gendenjamts, Ganbat Turbat, Tseveendorj Bayartsengel, Byambajav Tankhildulam, Dembee Unurzaya and director Ulamsain Ya of "Geo-Oron" company who were cooperated and helped to develop this manuscript. We also express our thanks to Professor Thomas K. Kelty for initiating our collaborative work with CSULB, where the oxygen isotope analysis was conducted. A respected friend and colleague of many scientists and geologists, Prof. Yin An remains in our memory, but his contribution to this manuscript is invaluable. We appreciate that he was supervisor of many professors, doctors in geology and structure geology. Blessed memory to him.

Conflicts of Interest: No.

References

1. Abdel-Rahman, A.F.M.; Nassar, P.E. Cenozoic volcanism in the Middle East: petrogenesis of alkali basalts from northern Lebanon. *Geol Mag* **2004,** *141,* 545–563, doi:10.1017/S0016756804009604.
2. Badarch, G.; Cunningham, W. D.; Windley, B. F. A new terrane subdivision for Mongolia: Implications for the Phanerozoic crustal growth of Central Asia. *J Asian Earth Sci* **2002**, *21*, 87–110, doi:10.1016/S1367-9120(02)00017-2.
3. Bailey, D.K. Continental rifting and mantle degassing, In *Petrology and geochemistry of continental rifts* / Ed. E.R. Neumann, I.B. Ramberg // Holland, Reidel, **1978**, 1-13.
4. Bussien, D.; Gombojav, N.; Winkler, W.; von Quadt, A. The Mongol-Okhotsk Belt in Mongolia-An Appraisal of the Geodynamic Development by the Study of Sandstone Provenance and Detrital Zircons. *Tectonophysics* **2011**, *510*, 132–150.
5. Collins, W.J.; Beams, S.D.; White, A. J. R.; Chappell, B. W. Nature and origin of A-type granites with particular reference to southeastern Australia. *Contrib Mineral Petrol* **982**, *2*, 189-200, doi:10.1007/BF00374895.
6. Cox, K. G. Continental Magmatic Underplating. *Philos Trans Roy Soc London* **1993**, *342*, 155-166, doi:10.1098/rsta.1993.0011. JSTOR 54188.
7. *Creaser, R.A.; Price, R.C.; Wormald, R.J.,* A-type granites revisited: assessment of a residual source model. *Geology* **1991**, *9*, 163-166, doi:10.1130/0091-7613(1991)019<0163**:** ATGRAO>2.3.CO;2.
8. Currie, K.L.; Eby, G.N.; Gittins J. The petrology of the Mount Saint Hilaire complex, southern Quebec: an alkaline gabbro-peralkaline syenite association. *Lithos* **1986,** *19*, 67-83, doi:10.1016/0024-4937(86)90016-2.
9. Dostal J.; Owen J.V.; Gerel O.; Keppie J.D.; Corney R.; Shellnutt J.G.; Macrae, A. The 186 Ma Dashbalbar alkaline granitoid pluton in the North Gobi rift of central Mongolia: evidence for melting of Neoproterozoic basement above a plume. *Amer J Sci* **2013**, *313*, 613-648, doi:10.2475/02.2014.06
10. Dostal J.; Owen J.V.; Shellnutt J.G.; Keppie J.D.; Gerel O.; Corney, R. Petrogenesis of the Triassic Bayan-Ulan alkaline granitic pluton in the North Gobi rift: implications of Early Mesozoic granitoid magmatism in the Central Asian Orogenic Belt. *J Asian Earth Sci* **2015,** *109*, 50-62, doi:10.1016/j.jseaes.2015.04.021.
11. Eby, G.N. The A-type granitoids: A review of their occurrence and chemical characteristics and speculations on their petrogenesis. *Lithos* **1990,** *26*, 115-134, doi:10.1016/0024-4937(90)90043-Z.
12. Eiler, J.M.; Farley, K.A.; Valley, J.W.; Hauri, E.; Craig, H.; Hart, S.R.; Stolper, E.M. Oxygen isotope variations in ocean island basalt phenocrysts. *Geochim Cosmochim Acta* **1997,** *61*, 2281-2293, doi:10.1016/S0016-7037(97)00075-6.
13. Ferre, E.C.; Galland, O.; *Montanari,* D.; Kalakay, T.J. *Granite magma* migration and emplacement along thrusts. *Int J Earth Sci* **2012**, *101*, 1673-1688, doi:10.1007/s00531-012-0747-6.
14. Enkhbat, Ts.; Baldorj, B.; Ulamsain, Ya.; Enksaikhan, Ch.; Otgonbayar, M. Geological mapping and preliminary prospecting project at scale of 1:50000 in Mungun Morit, Bayanjargalan areas of Tuv, and Tsenhermandal, Delgerkhan areas of Khentei province. *Open file report 8180* **2017,** Ulaanbaatar (in Mongolian)
15. Foland, K. A.; Allen, J. C. Magma Sources for Mesozoic Anorogenic Granites of the White Mountain Magma Series, New-England, USA. *Contrib Mineral Petrol* **1991**, *109*, 195-211.
16. Garamjav, D. The constructions of vortex process in earth. Ulaanbaatar **2007**, pp. 415-420 (In Mongolian)

17. Gröning, M. International stable isotope reference materials. In Handbook *of Stable Isotope Analytical Techniques.* Ed. P.A. De Groot I, **2004,** pp.874-906.
18. Harris, N.B.W.; Inger, S. Geochemical characteristics of pelite-derived granites. *Contrib Mineral Petrol* 1992**,** 110, 46-56.
19. Harris, N.B.W.; Marriner, G.F. Geochemistry and petrogenesis of a peralkaline granite complex from the Midian Mountains, Saudi Arabia. *Lithos* **1980,** *13,* 325-337.
20. Helo, C.; Hegner, E.; Kroner, A.; Badarch, G.; Tomurtogoo, O.; Windley, B.F.; Dulski, P. Geochemical signature of Paleozoic accretionary complexes of the Central Asian Orogenic Belt in South Mongolia: constraints on arc environments and crustal growth. *Chem Geol* **2006**, *227*, 236-257, doi: 10.1016/j.chemgeo.2005.10.003.
21. Hollocher, K. CIPW Norm Calculation Program. Geology Department, Union College, 2004.
22. Hong, D.W.; Zhang J.S.; Wang, T.; Wang, S.G.; Xilin, X. Continental crustal growth and the supercontinental cycle: Evidence from the Central Asian Orogenic Belt. *J Asian Earth Sci* **2004,** *23,* 799-813, doi: 10.1016/S1367-9120(03)00134-2.
23. Iizumi, S. Sr and Nd isotopic analyses, using a thermal ionization mass spectrometer MAT 262. *Geoscience report of Shimane University* **1996,** *15,* 153-159 (in Japanese with English abstract)
24. Iizumi, S.; Maehara, K.; Morris, P.A.; Sawada, Y. Sr isotope data of some GSJ rock reference samples. *Memories of the Faculty of Scence, Shimane University* **1994**, *28*, 83-36.
25. Jahn, B.; Wu, F.; Chen, B. Granitoids of the Central Asian Orogenic Belt and continental growth in the Phanerozoic. *Trans Roy Soc Edinb, Earth Sci* **2000**, *91,* 181- 193. doi:10.1130/0-8137-2350-7.181.
26. Kato, Y.; Fujinaga, K.; Nakamura, K.; Takaya, Y.; Kitamura, K.; Ohta, J.;Toda, R.; Nakashima, T.; Iwamori, H. Deep-sea mud in the Pacific Ocean as a potential resource for rare-earth elements. *Nature Geoscience* **2011**, *4*, 534–539.
27. Kimura, J.I.; Takaku, Y.; Yoshida. T. Igneous Rocks Analysis Using ICP-MC with internal Standardization, Isobaric ions overlaps correction, and standard addition method. *Scientific report Fukushima University* **1995**, *56*, 1-11.
28. Konstantinovskaia, E.; Malavieille, J. Erosion and exhumation in accretionary orogens: Experimental and geological approaches. *Geochem Geophys* **2005**, *6*, 17-25, doi:10.1029/2004GC000794.
29. Kovalenko, V.I.; Yarmolyuk, V.V.; Kozlovsky, A.M.; Kovach V.P.; Salnikova, E.B.; Kotov, A.B.; Vladykin, N.V. Two types of magma sources of rare-metal alkali granites. *Geology of ore deposits* **2007**, *49*, 506-534, doi:10.1134/S1075701507060025.
30. Kovalenko, V.I.; Yarmolyuk, V.V.; Salnikova, E.B.; Kozlovsky, A.M.; Kotov, A.B.; Kovach V.P.; Savatenkov, V.M.; Vladykin, N.V.; Ponomarchuk,V.A. Geology, geochronology, and geodynamics of the Khanbogd alkali granite pluton in Southern Mongolia. *Geotectonics* **2006,** *40,* 450-466 (In Russian)
31. Kovalenko, V.I.; Yarmolyuk, V.V.; Kovach, V.P.; Kotov, A.B.; Kozakov, I.K.; Salnikova, E.B.; Larin A.M. Isotope provinces, mechanisms of generation and sources of the continental crust in the Central Asian mobile belt: geological and isotopic evidence. *J Asian Earth Sci* **2004**, *23,* 605-627, doi:10.1016/S1367-9120(03)00130-5.
32. Kovalenko, V.I.; Kuzmin, M.I.; Zonenshain, L.P.; Nagibina, M.S.; Pavlenko, A.S.; Vladykin, N.V.; Tseden, Ts.; Gundsambuu, Ts.; Goreglyad, A.V. Rare metal granitoids in Mongolia: petrology, distribution of rare elements. *Nedra, Moscow* **1971**, p. 239 (in Russian)
33. Kozakov, I.K.; Kotov, A.B.; Kovach, V.P.; Salnikova, E.B. Crustal growth in the geologic evolution of the Baidarik Block, central Mongolia: Evidence from Sm-Nd isotopic systematics: *Petrology* **1997,** *5,* 201-207 (In Russia)
34. Kozlovsky, A.M.; Yarmolyuk, V.V.; Salnikova, E.B.; Travin, A.V.; Kotov, A.B.; Plotkina, J.V.; Kudryashova, E.A.; Savatenkov, V.M. Late Paleozoic anorogenic magmatism of the Gobi Altai (SW Mongolia): Tectonic position, geochronology and correlation with igneous activity of the Central Asian Orogenic Belt. *J Asian Earth Sci* **2015**, *113*, 524-541, doi: 10.1016/j.jseaes.2015.01.013.
35. Kozlovsky, A. M.; Yarmolyuk, V. V.; Salnikova, E. B.; Kovalenko, V.I. Age of Bimodal and Alkali Granite Magmatism of the Gobi–Tien Shan Rift Zone, Tost Range, southern Mongolia. *Petrology* **2005**, *13*, 197-203.
36. Kynicky J.; Chakhmouradian A.R.; Xu C.; Krmicek L.; Galiova M. Distribution and evolution of zirconium mineralization in peralkaline granites and associated pegmatites of the Khan Bogd complex, Southern Mongolia. *Canad Mineral* **2011,** *49,* 947-965, doi*: 10.3749/canmin.49.4.947*.
37. Loiselle, M.C.; Wones, D.R. Characteristics of anorogenic granites. *Geol Soc Am Bull* **1979**, *11,* 468.
38. Malavieille, J. Impact of erosion, sedimentation, and structural heritage on the structure and kinematics of orogenic wedges: Analog models and case studies. *GSA Today* **2010**, *20,* 4-10, doi:10.1130/GSATG48A.1.
39. Magaritz, M.; Whitford, D.J.; James, D.E. Oxygen isotopes and the origin of high Sr/Sr andesites. *Earth Planet Sci Lett* **1978**, *40,* 200-230, doi:10.1016/0012-821X (78)90092-4.
40. Milinovic, J.; Rodrigues, F.J.L.; Barriga, F.J.A.S.; Murton, B.J. Ocean-Floor Sediments as a Resource of Rare Earth Elements: An Overview of Recently Studied Sites. *Minerals* **2021**, *11,* 142, doi:10.3390/min11020142.

41. Nowell, G.M.; Kempton, P.D.; Noble, S.R.; Fitton, J.G.; Saunders, A.D.; Mahoney, J.J.; Taylor, R.N. High precision Hf isotope measurements of MORB and OIB by thermal ionisation mass spectrometry: insights into the depleted mantle. *Chem Geol* 1998, *149,* 211-233, doi:10.1016/S0009-2541(98)00036-9.
42. Othman, D. B.; White, W.M.; Patchett, J. The geochemistry of marine sediments, island arc magma genesis, and crust -mantle recycling. *Earth Planet Sci Lett* **1989**, *94*, 1-21, doi:10.1016/0012-821X(89)90079-4.
43. Patchett, P.J. Isotopic studies of Proterozoic crustal growth and evolution. In *Proterozoic crustal evolution.* Ed. K.C. Condie, Elsevier Science Amsterdam **1992**, pp. 481-508.
44. Patino Douce, A.E. Vapor-Absent Melting of Tonalite at 15-32 kbar. *J Petrol* **2005,** *46*, 275-290, doi:10.1093/petrology/egh071.
45. Pearce, J. A. The role of sub-continental lithosphere in magma genesis at destructive plate margins, In *Continental Basalts and Mantle Xenoliths: Nantwich, Shiva.* Eds. C.J. Hawkesworth, M. J. Norry. **1983**, pp. 230-249.
46. Petford, N. Structure and Emplacement of high-level magmatic systems. In *Geological Society, London, Special Publications*. Eds. K.Thomson, N. Petroford. **2008**, *302,* pp.1-2.
47. Plank, T.; Langmuir, C.H. The chemical composition of subducting sediment and its consequences for the crust and mantle. *Chem Geol* **1998,** *145,* 325-394, doi:10.1016/S0009-2541(97)00150-2.
48. Serjlkhumbe, A. U- Pb geochronology and multi-isotopic systematics of granitoids from Mongolia, Central Asian orogenic belt: implications for granitoid origin and crustal growth during the Phanerozoic. Doctoral thesis **2008**, Okayama University Japan.
49. Serjlkhumbe, A. Petrological and geochemical studies on the Khanbogd alkaline complex, South Mongolia. Master course thesis **2004,** Shimane University, Japan.
50. Shand, S. J. The Eruptive Rocks. 2 ed. New York, *John Wiley Publishers* **1943,** 444 p.
51. Sharp. Z.D.; Atudorei, V.; Durakeiwicz, T. A rapid method for determination of hydrogen and oxygen isotope ratios from water and hydrous minerals. *Chem Geol* **2001,** *178,* 197-210, doi:10.1016/S0009-2541(01)00262-5.
52. Sharp, Z. D. A laser-based microanalytical method for the insitu determination of oxygen iso tope ratios of silicates and oxides. *Geochim Cosmochim Acta* **1990,** *54,* 1353-1357, doi:10.1016/0016-7037(90)90160-M.
53. Skjerlie, K.P.; Jonston, A.D. Vapor-absent melting at 10 kbar of a biotite- and amphibole-bearing tonalitic gneiss: Implications for the generation of A-type granites. *Geology* **1992,** *20,* 263-266, doi:10.1130/0091-7613(1992)020<0263: VAMAKO> 2.3.CO;2.
54. Sun, S.; McDonough, W.F. Chemical and isotopic systematics of oceanic basalts: implications for mantle composition and processes, In *Magmatism in the Ocean Basins.* Eds. A.D. Saundrers, M.J. Norry, Geological Society of London. Special Publications **1989,** 42, pp. 313-345.
55. Takaya, Y.; Yasukawa, K.; Kawasaki, T.; Fujinaga, K.; Ohta, J.; Usui, Y.; Nakamura, K.; Kimura, J.I.; Chang, Q.; Hamada, M.; Dodbiba, G. et al. The tremendous potential of deep-sea mud as a source of rare-earth elements. *Scientific Reports* **2018**, *8,* 5763.
56. Tayler, H. P. Jr.; Epstein, S. Oxygen Isotope Studies on the Origin of Tektites. *J Geophys Res* **1962,** *67,* 4485-4490, doi:10.1029/JZ067i011p04485.
57. Thomson, K.; Schofield, N. Lithological and structural controls on the emplacement and morphology of sills in sedimentary basins. *GSL, Special Publications,* **2008,** 302, 31-44. doi:10.1144/SP302.3
58. Thybo, H.; Nielsen, C. A. Magma-compensated crustal thinning in continental rift zones. *Nature,* **2009,** *457,* 873– 876, doi: 10.1038/nature07688.
59. Tong, Y.; Jahn, B.M.; Wang, T.; Hong, D.W.; Smith, E.I.; Sun, M.; Gao, J.F.; Yang, Q.D.; Huang, W. Permian alkaline granites in the Erenhot–Hegenshan belt, northern Inner Mongolia, China: Model of generation, time of emplacement and regional tectonic significance. *J Asian Earth Sci* **2015**, *97* (part B), 320-336, doi:10.1016/j.jseaes.2014.10.011.
60. Vervoort, J.D.; Patchett, P.J.; Toft, J.B.; Albarede. F. Relationships between Lu–Hf and Sm–Nd isotopic systems in the global sedimentary system. *Earth Planet Sci Lett* **1999**, *168*, 79-99, doi:10.1016/S0012-821X(99)00047-3.
61. Vervoort, J.D.; Patchett, P.J. Behavior of hafnium and neodymium isotopes in the crust: Constraints from Precambrian crustally derived granites**.** *Geochim Cosmochim Acta* **1996,** *60,* 3717-3733, doi:10.1016/0016-7037(96)00201-3.
62. Vladykin, N.V.; Drits, V.A.; Kovalenko, V.I.; Dorfman, M.D.; Malov, V.S.; Gorshkov, A.I. A new silicate of niobium, mongolite $Ca_4Nb_6[Si_5O_{20}]O_4(OH_{10})$ $^2nH_2O$: *Zap. Vses. Mineral. Obshch*., **1985,** 114, 374-377, (in Russian)
63. Vladikin N.B.; Kovalenko V.I.; Dorfman M.D. Mineralogical and geochemical characteristics of Khanbogd peralkaline granite pluton: Moscow, *Nauka* **1981,** pp.3-135 (In Russian)
64. Vladykin, N.V.; Kovalenko, V.I.: Kashaev, A.A.; Sapozhnikov, A.N.; Pisarskaya, V.A. A new silicate of calcium and zirconium – armstrongite. *Doklady Akademii Nauk SSSR* **1973,** *209*, 1185-1188 (In Russian)
65. Whalen, J.B.; Currie, K.L.; Chappel, B.W. A-type granites: geochemical characteristics, discrimination and petrogenesis. *Contrib Mineral* **1987**, *95,* 407-419.

66. Whitney, D.L.; Evans, B.W. Abbreviations for names of rock-forming minerals. *Amer Miner* **2010,** *95,* 185–187, doi:10.2138/am.2010.3371.
67. Wilson, P.I.R.; McCaffrey, K.J.W; Wilson, R.W.; Jarvis, I.; and Holdsworth, R.E. Deformation structure associated with the Trachyte Mesa intrusion, Henry Mountains, Utah: Implications for sill and laccolith emplacement mechanism. *J Struct Geol* **2016,** *87*, 30-46, doi:10.1016/j.jsg.2016.04.001.
68. Yanshin. A.L. Ed. Geological Formations Map of Mongolian People's Republic at a scale of 1:1 500 000. Moscow, *Nedra* **1989** (In Russian)
69. Yasukawa, K.; Liu, H.; Fujinaga, K.; Machida, S.; Haraguchi, S.; Ishii, T.; Nakamura, K.; Kato, Y. Geochemistry and mineralogy of REY-rich mud in the eastern Indian Ocean. *J Asian Earth Sci* **2014**, *93*, 25-36, doi:10.1016/j.jseaes.2014.07.005.
70. Yarmolyuk, V.V.; Kovalenko, V.I.; Salnikova, E.B.; Kovach, V.P.; Kozlovsky, A.M.; Kotov, A. B.; Lebedev, V.I. Geochronology of igneous rocks and formation of the Late Paleozoic South Mongolian Active Margin of the Siberian Continent. *Stratigraphy and Geological Correlation* **2008,** *16,* 162-181.
71. Zartman, R.E.; Doe, B.R. Plumbotectonics-the model. *Tectonophysics* **1981**, *75*, 135-162, doi:10.1016/0040-1951(81)90213-4.
72. Zhang, X.; Gao, Y.; Lei Sh. Geochronology and Geochemistry of the Early Permian A-type Granite in the Hongol Area, Central Inner Mongolia: Petrogenesis and Tectonic Implications. *Acta Geol Sin* **2018,** *92*, 988-1007, doi:10.1111/1755-6724.13587.
73. Zhao, Z.; Xiong, X.; Wang, Q.; Bai, Z.; Qiao, Y. Late Paleozoic underplating in North Xinjiang: Evidence from shoshonites and adakites. *Gondwana Res* **2009**, *16*, 216-226, doi.org/10.1016/j.gr.2009.03.001.